explosions, make a definitive measurement of the primordial lithium abundance (which strongly constrains 'big bang' nucleosynthesis)[28], and obtain tighter constraints on the nature of the FMF. If any examples of the so-called r-process-enhanced stars are found with [Fe/H] < -4.0, we may be able to use nucleochronometry[29] to obtain a direct estimate of the epoch of first star formation in the Universe, possibly resulting in an improved lower limit for the age of the Universe. □

Received 1 July; accepted 24 September 2002; doi:10.1038/nature01142.

1. Norris, J. E., Ryan, S. G. & Beers, T. C. Extremely metal-poor stars. VIII. High-resolution, high signal-to-noise ratio analysis of five stars with [Fe/H] < -3.5. *Astrophys. J.* **561,** 1034–1059 (2001).
2. Cohen, J. G., Christlieb, N., Beers, T. C., Gratton, R. & Carretta, E. Stellar archaeology: A Keck pilot program on extremely metal-poor stars from the Hamburg/ESO survey. I. Stellar parameters. *Astron. J.* **124,** 470–480 (2002).
3. Bond, H. E. Where is population III? *Astrophys. J.* **248,** 606–611 (1981).
4. Beers, T. C. in *The Third Stromlo Symposium: The Galactic Halo* (eds Gibson, B. K., Axelrod, T. S. & Putman, M. E.) *Astron. Soc. Pacif. Conf. Ser.* **165**, 202–212 (1999).
5. Bromm, V., Ferrara, A., Coppi, P. S. & Larson, R. B. The fragmentation of pre-enriched primordial objects. *Mon. Not. R. Astron. Soc.* **328,** 969–976 (2001).
6. Schneider, R., Ferrara, A., Natarajan, P. & Omukai, K. First stars, very massive black holes, and metals. *Astrophys. J.* **571,** 30–39 (2002).
7. Wisotzki, L. *et al.* The Hamburg/ESO survey for bright QSOs. III. A large flux-limited sample of QSOs. *Astron. Astrophys.* **358,** 77–87 (2000).
8. Christlieb, N. *et al.* The stellar content of the Hamburg/ESO survey. I. Automated selection of DA white dwarfs. *Astron. Astrophys.* **366,** 898–912 (2001).
9. Yi, S. *et al.* Towards better age estimates for stellar populations: The Y^2 isochrones for solar mixture. *Astrophys. J. Suppl.* **136,** 417–437 (2001).
10. Mathis, J. S. & Lamers, H. J. G. L. M. The origin of the extremely metal-poor post-AGB stars. *Astron. Astrophys* **259,** L39–L42 (1992).
11. Van Winckel, H., Waelkens, C. & Waters, L. B. F. M. The extremely iron-deficient "post-AGB" stars and binaries. *Astron. Astrophys.* **293,** L25–L28 (1995).
12. Waters, L. B. F. M., Trams, N. R. & Waelkens, C. A scenario for the selective depletion of stellar atmospheres. *Astron. Astrophys.* **262,** L37–L40 (1992).
13. Bakker, E. J. *et al.* The optical spectrum of HR 4049. *Astron. Astrophys.* **306,** 924–934 (1996).
14. Woosley, S. E. & Weaver, T. A. The evolution and explosion of massive stars. II. Explosive hydrodynamics and nucleosynthesis. *Astrophys. J.* **101,** 181–235 (1995).
15. Yoshii, Y. Metal enrichment in the atmospheres of extremely metal-deficient dwarf stars by accretion of interstellar matter. *Astron. Astrophys.* **97,** 280–290 (1981).
16. McClure, R. D. & Woodsworth, A. W. The binary nature of the Barium and CH stars. III. Orbital parameters. *Astrophys. J.* **352,** 709–723 (1990).
17. Fujimoto, M. Y., Ikeda, Y. & Iben, I. Jr The origin of extremely metal-poor carbon stars and the search for population III. *Astrophys. J.* **529,** L25–L28 (2000).
18. Schlattl, H., Salaris, M., Cassisi, S. & Weiss, A. The surface carbon and nitrogen abundances in models of ultra metal-poor stars. *Astron. Astrophys.* (2002) (in the press); also preprint astro-ph/0205326 at ⟨http://xxx.lanl.gov⟩.
19. Siess, L., Livio, M. & Lattanzio, J. Structure, evolution, and nucleosynthesis of primordial stars. *Astrophys. J.* **570,** 329–343 (2002).
20. Norris, J., Ryan, S. G. & Beers, T. C. Extremely metal poor stars. The carbon-rich, neutron capture element-poor object CS 22957−027. *Astrophys. J.* **489,** L169–L172 (1997).
21. Aoki, W., Norris, J. E., Ryan, S. G., Beers, T. C. & Ando, H. The chemical composition of carbon-rich, very metal poor stars: a new class of mildly carbon rich objects without excess of neutron-capture elements. *Astrophys. J.* **567,** 1166–1182 (2002).
22. Yoshii, Y. & Sabano, Y. Stability of a collapsing pre-Galactic gas cloud. *Publ. Astron. Soc. Jpn* **31,** 505–521 (1979).
23. Palla, F., Salpeter, E. E. & Stahler, S. W. Primordial star formation: the role of molecular hydrogen. *Astrophys. J.* **271,** 632–641 (1983).
24. Gass, H., Liebert, J. & Wehrse, R. Spectrum analysis of the extremely metal-poor carbon dwarf star G77-61. *Astron. Astrophys.* **189,** 194–198 (1988).
25. Yoshii, Y. & Saio, H. Initial mass function for zero-metal stars. *Astrophys. J.* **301,** 587–600 (1986).
26. Nakamura, F. & Umemura, M. On the initial mass function of population III stars. *Astrophys. J.* **548,** 19–32 (2001).
27. Ostriker, J. P. & Gnedin, N. Y. Reheating of the universe and population III. *Astrophys. J.* **472,** L63–L67 (1996).
28. Ryan, S. G., Norris, J. E. & Beers, T. C. The Spite lithium plateau: ultrathin but postprimordial. *Astrophys. J.* **523,** 654–677 (1999).
29. Cayrel, R. *et al.* Measurement of stellar age from uranium decay. *Nature* **409,** 691–692 (2001).

Acknowledgements We thank the European Southern Observatory for providing us with reduced UVES spectra. We are grateful to M. Asplund, B. Edvardsson, J. Lattanzio, J. Norris, N. Piskunov, B. Plez, D. Reimers, S.G. Ryan, L. Siess and L. Wisotzki for their contributions and suggestions. N.C. acknowledges a Marie Curie Fellowship granted by the European Commission, and support from Deutsche Forschungsgemeinschaft. T.C.B. acknowledges grants of the US National Science Foundation, S.R. support from FAPESP and CNPq, and the Uppsala group from the Swedish Research Council.

Competing interests statement The authors declare that they have no competing financial interests.

Correspondence and requests for materials should be addressed to N.C. (e-mail: nchristlieb@hs.uni-hamburg.de).

Measurement of the conductance of a hydrogen molecule

R. H. M. Smit*, Y. Noat*†, C. Untiedt*, N. D. Lang‡, M. C. van Hemert§ & J. M. van Ruitenbeek*

* *Kamerlingh Onnes Laboratorium, Universiteit Leiden, PO Box 9504, 2300 RA Leiden, The Netherlands*
‡ *IBM Research Division, Thomas J. Watson Research Center, Yorktown Heights, New York 10598, USA*
§ *Leids Instituut voor Chemisch Onderzoek, Gorlaeus Laboratorium, Universiteit Leiden, PO Box 9502, 2300 RA Leiden, The Netherlands*

Recent years have shown steady progress towards molecular electronics[1,2], in which molecules form basic components such as switches[3–5], diodes[6] and electronic mixers[7]. Often, a scanning tunnelling microscope is used to address an individual molecule, although this arrangement does not provide long-term stability. Therefore, metal–molecule–metal links using break-junction devices[8–10] have also been explored; however, it is difficult to establish unambiguously that a single molecule forms the contact[11]. Here we show that a single hydrogen molecule can form a stable bridge between platinum electrodes. In contrast to results for organic molecules, the bridge has a nearly perfect conductance of one quantum unit, carried by a single channel. The hydrogen bridge represents a simple test system in which to understand fundamental transport properties of single-molecule devices.

Here we use a mechanically controllable break junction[12,13] at low temperatures (4.2 K) to produce pure metallic contacts of atomic size. Figure 1 inset shows a typical conductance curve for a clean Pt contact that was recorded while gradually decreasing the contact size by increasing the piezovoltage (black curve). (We concentrate here on results obtained for Pt wires, but conductance histograms suggest similar behaviour for Pd.) The conductance is expressed in terms of the quantum unit, $G_0 = 2e^2/h$, with e the electron charge and h Planck's constant. The jumps in conductance are the result of sudden atomic rearrangements in response to the applied strain[14]. After the conductance has dropped to a value corresponding to a single atom—which for Pt is in the range 1.2–2.3G_0—the contact suddenly breaks. In order to extract the common features of these conductance curves, we collect the data of a large series of conductance curves into a conductance histogram. The main panel in Fig. 1 shows such a histogram for Pt contacts (black). It is dominated by a large peak at 1.4–1.8G_0, which represents the range of conductance values for contacts having a single atom in cross-section (for a recent review, see ref. 15). The histogram drops sharply to zero for lower conductance values, as is typically found for Pt contacts in the absence of adsorbates and impurities.

The character of the conductance curves and the shape of the resulting histogram change markedly when a small quantity of hydrogen gas is admitted to the vacuum vessel (grey curves). The critical amount is difficult to establish, as most hydrogen is expected to condense on the walls of the container (the equilibrium H_2 gas pressure at a temperature of 4.2 K is about 10^{-6} mbar), but the results are not very sensitive to the precise quantity. The peak at the position characteristic for Pt disappears, and a large weight is added in the entire range below that value. On top of this background a distinct peak close to $1G_0$ is found, which grows for larger currents through the contact, while the background is suppressed. For still larger bias voltages, above 200 mV, we recover the histogram for clean Pt. The low-conductance tail and the peak at $1G_0$ reappear

† Present address: Université Denis Diderot (Paris 7), Groupe de Physique des Solides UMR 75 88, 2 place Jussieu, 75251 Paris Cedex 05, France.

 © 2002 Nature Publishing Group

upon lowering the bias again. The bias dependence of the histograms is attributed to local heating by the current. For moderate bias the weakly bound physisorbed H_2 is evaporated, and only above 200 mV the chemically bonded hydrogen molecules are removed from the Pt surface.

We concentrate now on the fact that in the presence of hydrogen there appears to be a frequently occurring stable configuration that has a conductance of nearly unity, an example of which is shown in Fig. 1 inset, and which is responsible for the sharp peak just below $1G_0$ in the histogram. We can select this configuration by recording conductance traces of the type shown in the inset, and stop the motion of the electrodes as soon as we find a plateau at $\sim 1G_0$. In order to investigate the structure of the contact on this plateau we use point contact spectroscopy. This technique was originally developed[16,17] for contacts that are large compared to the atomic scale. The differential conductance, $G_d(V) = dI/dV$, is measured as a function of the d.c. bias voltage. The electrons in the contact are accelerated to an excess energy eV. When this energy reaches that of the main phonon modes of the metal, inelastic scattering results in an enhanced probability for the electrons to scatter back through the contact, which is seen as a drop in $G_d(V)$. This principle has recently been applied to single-atom metallic contacts and chains of atoms[18,19], and a theoretical description for localized vibration modes in quantum point contacts has been developed[20,21]. Vibration modes for individual molecules have been observed before, using inelastic electron tunnelling spectroscopy (IETS) in a low-temperature scanning tunnelling microscope[22]. Although the principle is similar, the conductance increases at the vibration energy in IETS, whereas it decreases in point contact spectroscopy. Experimentally, a great advantage is the short data acquisition time for a spectrum in our experiment, 10 s compared to 1–10 h for IETS[22]. This is attributed mainly to a lower shot noise level as result of the lower resistance of the junction, and due to the quantum suppression of shot noise for a single-channel contact[23]; the lower junction impedance also allows us to work at a higher modulation frequency.

Figure 2 shows the differential conductance and its derivative taken at a $1G_0$-plateau for the Pt/H_2 system. We find a pronounced single resonance at about 63.5 mV, symmetrically for both voltage polarities. The energy is much higher than the typical phonon modes for metals, which are found[24] between 5 and 25 mV. The width of the resonance is about 14 mV, and is much larger than expected from the thermal and instrumental broadening. A similar large 'intrinsic width' has been observed in IETS[22], and it probably results from the short lifetime of the molecular vibration excitations owing to the strong coupling to the metal. We observe a modest variation in the position of the main signal between different experiments, which is probably due to variations in the bonding configuration of the hydrogen to the Pt electrodes. The frequencies obtained from 23 spectra for Pt/H_2 are shown by the open circles in Fig. 3, having a mean value of 64 mV and a standard deviation of 4 mV.

In order to test the interpretation of the observed resonance, we repeated the experiment using the isotopes D_2 and HD. From 23 spectra for Pt/D_2 we obtain a distribution of energies shown by open squares in Fig. 3, being centred at 47 mV, while 20 spectra obtained for Pt/HD (filled circles) are found to be centred at 51 mV. Figure 3 inset shows the same distributions with energies scaled by the expected ratios for the vibration energies $\omega_{H_2}/\omega_{D_2} \propto \sqrt{m_{D_2}/m_{H_2}} = \sqrt{2} \approx 1.414$, and $\omega_{H_2}/\omega_{HD} \propto \sqrt{m_{HD}/m_{H_2}} = \sqrt{3/2} \approx 1.225$, confirming our interpretation of the conduction through a hydrogen molecule. Note in particular that this excludes the possibility of conductance through a hydrogen atom, as this would have resulted in a two-peak distribution of frequencies for HD.

Experimental information on the number of conductance modes can be obtained from the fluctuations in $G_d(V)$ as a function of

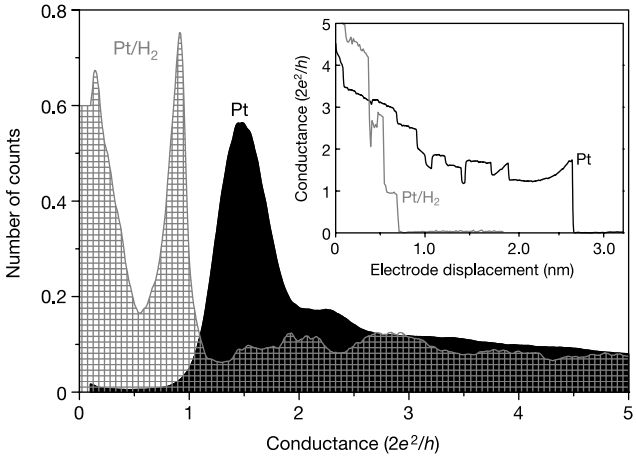

Figure 1 Conductance curves and histograms for clean Pt, and for Pt in a H_2 atmosphere. Inset, a conductance curve for clean Pt (black line) at 4.2 K recorded with a bias voltage of 10 mV, before admitting H_2 gas into the system. About 10,000 similar curves are used to build the conductance histogram shown in the main panel (black), which has been normalized by the area under the curve. After introducing H_2 gas, the conductance curves change qualitatively as illustrated by the grey curve in the inset, recorded at 100 mV. This is most clearly brought out by the conductance histogram (grey; recorded with 140 mV bias). Briefly, the mechanically controllable break-junction technique works as follows. Starting with a macroscopic metal wire, a notch is formed by incision with a knife. The samples are mounted inside a vacuum container and pumped to a pressure below 5×10^{-7} mbar. Next, the system is cooled to 4.2 K in order to attain a cryogenic vacuum. After cooling, the sample wire is broken at the notch by bending of the substrate onto which it has been fixed. The clean, freshly exposed fracture surfaces are then brought back into contact by slightly relaxing the bending. With the use of a piezoelectric element, the displacement of the two electrodes can be finely adjusted to form a stable contact of atomic size. A thick copper finger provides thermal contact to the sample inside the container.

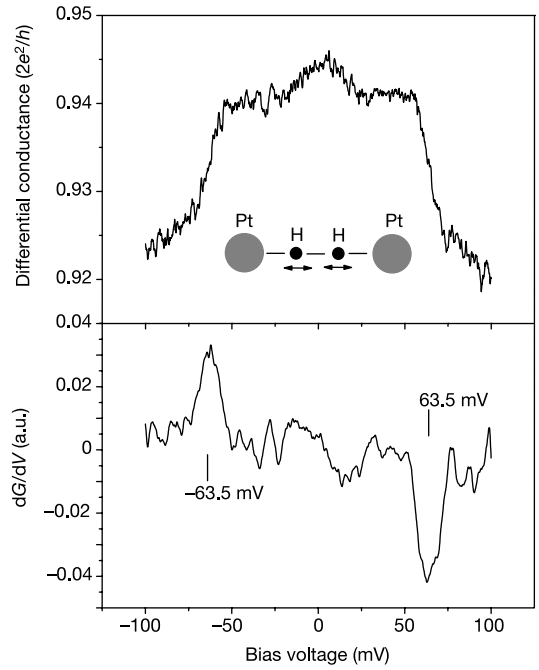

Figure 2 Differential conductance (top) and its derivative (bottom) for a Pt/H_2 contact taken at a conductance plateau close to $1G_0$. The differential conductance is recorded by a lock-in amplifier using a modulation amplitude between 0.88 and 1.5 mV_{rms} at 7 kHz and a time constant of 10 ms, and the derivative is numerically calculated. A full spectrum is recorded in 10 s.

© 2002 Nature Publishing Group

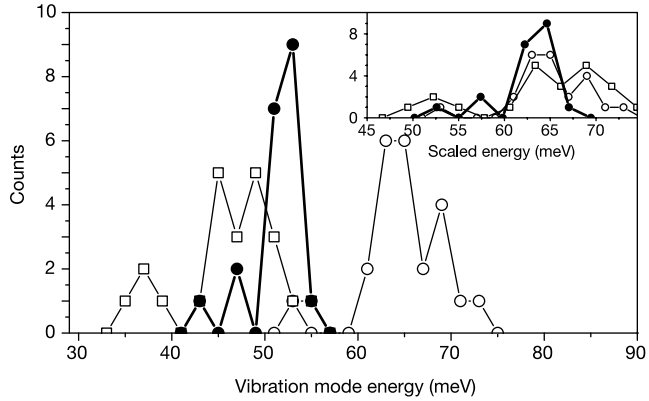

Figure 3 Vibration mode energies obtained from point contact spectra similar to that shown in Fig. 2. Open circles, Pt/H_2; open squares, Pt/D_2; filled circles, Pt/HD. The vertical scale shows the number of spectra with energies within a bin size of 2 meV. The inset shows the same data with the energy axis scaled by the factors expected for the isotope shifts of the hydrogen molecule, $\omega_{H_2}/\omega_{D_2} \propto \sqrt{m_{D_2}/m_{H_2}} = \sqrt{2} \approx 1.414$ (open squares), and $\omega_{H_2}/\omega_{HD} \propto \sqrt{m_{HD}/m_{H_2}} = \sqrt{3/2} \approx 1.225$ (filled circles).

voltage by measuring their root-mean-square (r.m.s.) amplitude σ_{GV} following the method described in ref. 25. For a contact with a single conductance channel with transmission probability $T < 1$, the dominant contribution to the fluctuations results from interference of partial waves reflected at the contact itself and those reflected on defects nearby. The wavelength of the electrons changes as a function of the bias voltage, producing random variations in the interference and thus in the conductance. For $T = 1$ the reflection at the contact vanishes, resulting in a suppression of the fluctuations. The peak in the conductance histogram at $0.95G_0$ coincides with a pronounced minimum in σ_{GV} (Fig. 4). From the finite value of σ_{GV} at the minimum[25], we extract a value for the transmission $T = 0.97 \pm 0.01$, confirming that the conductance through the molecule is almost entirely carried by one channel. This finding also excludes other configurations for which the conductance would be carried through several parallel channels, and confirms that we have only a single molecule.

Hydrogen is known to bind strongly to a Pt surface, and Pt surfaces catalyse hydrogen dissociation. Little is known about the catalytic activity of this system at 4.2 K, but it is likely that a small energy barrier is present that prevents H_2 dissociation. In our experiment we cannot rule out the formation of contacts with atomic hydrogen, but the ones that we have been able to fully analyse have a molecular bridge. We have verified the stability of the H_2-bridge configuration using density functional calculations employing the Gaussian 98 program[26] with the SDD relativistic effective core basis set[27] and the B3LYP functional[28]. Calculations were performed starting with a linear chain of four Pt atoms, and the results were verified to be insensitive to adding more atoms to the length of the Pt chain. Performing first-principles molecular dynamics calculations, we find that a H_2 molecule bonded to the side of a Pt chain spontaneously moves as a whole into the chain when the bonds between the Pt atoms are being stretched. The energy gain is 2.0 eV, as compared to free H_2 and two Pt_2 chain fragments at infinity. The binding energy of the Pt atoms in the chain is 2.75 eV per bond. H_2 will therefore never move spontaneously into the chain, but first requires an external force to stretch a Pt–Pt bond, which is a way to supply chemical energy to a single bond. In order to obtain the longitudinal vibrational modes of H_2 in a Pt chain, we have explicitly calculated the potential energy curves. For the centre of mass motion of H_2 we obtain an excitation energy of 61.5 meV, using equilibrium bond distances in a linear arrangement of 0.08 nm and 0.21 nm for H–H and Pt–H, respectively. This vibration mode fits very closely the observed excitation energy. The internal vibration mode of H_2 is too high in energy ($\sim$430 meV) to be observed in the experiment, as the contact becomes unstable at bias voltages above about 200 mV.

The conductance of the hydrogen bridge was calculated using a model of a chain of Pt–H–H–Pt, sandwiched between two 'jellium' bulk electrodes. We refer to ref. 29 for more details on the computation method. For the equilibrium bond distances we find a conductance of $0.9G_0$, in close agreement with experiment. We have not attempted to obtain the eigenchannel decomposition of the conductance.

The conduction through the molecule involves mainly the H_2 antibonding states, but the hybridization with the Pt metal states is strong enough to largely fill the gap between the highest occupied molecular orbital and the lowest unoccupied molecular orbital. It is surprising that the closed-shell configuration of H_2 permits such strong bonding with Pt, while the molecular character is largely conserved. The latter is shown by the calculated H–H bond distance, which is close to that of the free molecule, and the fact that in the simulations the bridge finally breaks at the Pt–H bond on further stretching. A Pt one-atom contact is expected to have five conductance channels owing to the partially occupied *d* orbitals. It

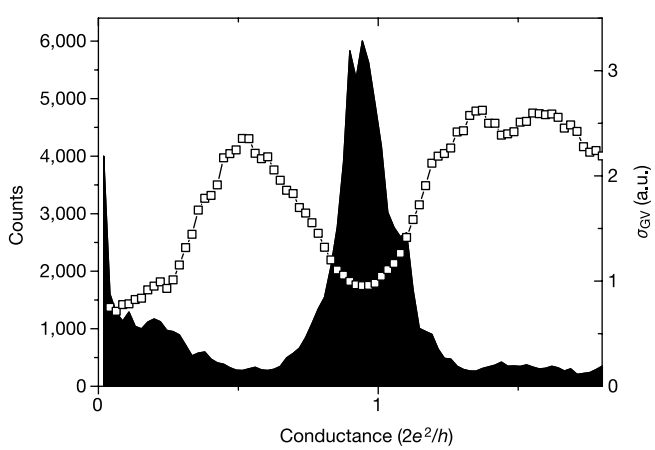

Figure 4 Conductance histogram (black, left axis) and r.m.s. amplitude of the conductance fluctuations σ_{GV} (open squares, right axis) for a Pt/H_2 sample. These data were obtained using 2,000 cycles of contact breaking. The conductance and its derivative were measured with two parallel lock-in amplifiers, detecting the frequencies *f* and 2*f*, with 140 mV bias voltage and 20 mV modulation amplitude. The derivative signal is used to calculate the average of the conductance fluctuations, σ_{GV}, and each of the points is obtained from the data belonging to one bin of the histogram.

© 2002 Nature Publishing Group

appears that the insertion of a hydrogen molecule has the effect of filtering out one of these five channels, with nearly perfect transmission.

It would be interesting to attempt to extend our technique to more complex molecules with built-in functional groups. Although most organic molecules are expected to have a conductance many orders of magnitude below the quantum unit, our experiments confirm[30] that full transmission of a single channel is possible when the coupling to the leads is sufficiently strong. Very recently, two groups have demonstrated conductance through single metal–organic molecules[31,32], for which the charge state of the metal ions could even be controlled by a gate electrode. Instead of using mechanical adjustment of the contact size as in our experiments, the size of the metal contacts to the molecule was reduced by exploiting electromigration. The tools needed to study and control electron transport at the single-molecule level are being rapidly developed. □

Received 8 May; accepted 29 August 2002; doi:10.1038/nature01103.

1. Aviram, A. & Ratner, M. (eds) *Molecular Electronics: Science and Technology* (Annals of the New York Academy of Sciences, New York, 1998).
2. Langlais, V. J. *et al.* Spatially resolved tunneling along a molecular wire. *Phys. Rev. Lett.* **83,** 2809–2812 (1999).
3. Gao, H. J. *et al.* Reversible, nanometer-scale conductance transitions in an organic complex. *Phys. Rev. Lett.* **84,** 1780–1783 (2000).
4. Collier, C. P. *et al.* Electronically configurable molecular-based logic gates. *Science* **285,** 391–394 (1999).
5. Reed, M. A., Chen, J., Rawlett, A. M., Price, D. W. & Tour, J. M. Molecular random access memory cell. *Appl. Phys. Lett.* **78,** 3735–3737 (2001).
6. Metzger, R. M. & Cava, M. P. in *Molecular Electronics: Science and Technology* (eds Aviram, A. & Ratner, M.) 95–115 (Annals of the New York Academy of Sciences, New York, 1998).
7. Chen, J., Reed, M. A., Rawlett, A. M. & Tour, J. M. Large on-off ratios and negative differential resistance in a molecular electronic device. *Science* **286,** 1550–1552 (1999).
8. Reed, M. A., Zhou, C., Muller, C. J., Burgin, T. P. & Tour, J. M. Conductance of a molecular junction. *Science* **278,** 252–254 (1997).
9. Kergueris, C. *et al.* Electronic transport through a metal-molecule-metal junction. *Phys. Rev. B* **59,** 12505–12513 (1999).
10. Reichert, J. *et al.* Driving current through single organic molecules. *Phys. Rev. Lett.* **88,** 176804 (2002).
11. Emberly, E. G. & Kirczenow, G. Comment on "First-principles calculation of transport properties of a molecular device". *Phys. Rev. Lett.* **87,** 269701 (2001).
12. Muller, C. J., van Ruitenbeek, J. M. & de Jongh, L. J. Experimental observation of the transition from weak link to tunneljunction. *Physica C* **191,** 485–504 (1992).
13. van Ruitenbeek, J. M. in *Mesoscopic Electron Transport* (eds Sohn, L. L., Kouwenhoven, L. P. & Schön, G.) 549–579 (Kluwer Academic, Dordrecht, 1997).
14. Rubio, G., Agraït, N. & Vieira, S. Atomic-sized metallic contacts: mechanical properties and electronic transport. *Phys. Rev. Lett.* **76,** 2302–2305 (1996).
15. Agraït, N., Levy Yeyati, A. & van Ruitenbeek, J. M. Quantum properties of atomic-sized conductors. Preprint cond-mat/0208239 at ⟨http://xxx.lanl.gov⟩ (2002).
16. Yanson, I. K. Nonlinear effects in the electric conductivity of point junctions and electron-phonon interaction in metals. *Zh. Eksp. Teor. Fiz.* **66,** 1035–1050 (1974); *Sov. Phys. JETP* **39,** 506–513 (1974).
17. Jansen, A. G. M., van Gelder, A. P. & Wyder, P. Point-contact spectroscopy in metals. *J. Phys. C* **13,** 6073–6118 (1980).
18. Untiedt, C., Rubio Bollinger, G., Vieira, S. & Agraït, N. Quantum interference in atomic-sized point-contacts. *Phys. Rev. B* **62,** 9962–9965 (2000).
19. Agraït, N., Untiedt, C., Rubio-Bollinger, G. & Vieira, S. Onset of dissipation in ballistic atomic wires. *Phys Rev. Lett.* **88,** 216803 (2002).
20. Bonča, J. & Trugman, S. A. Effect of inelastic processes on tunneling. *Phys. Rev. Lett.* **75,** 2566–2569 (1995).
21. Emberly, E. G. & Kirczenow, G. Landauer theory, inelastic scattering and electron transport in molecular wires. *Phys. Rev. B* **61,** 5740–5750 (1999).
22. Stipe, B. C., Rezaei, M. A. & Ho, W. Single-molecule vibrational spectroscopy and microscopy. *Science* **280,** 1732–1735 (1998).
23. van den Brom, H. E. & van Ruitenbeek, J. M. Quantum suppression of shot noise in atomic-size metallic contacts. *Phys. Rev. Lett.* **82,** 1526–1529 (1999).
24. Khotkevich, A. V. & Yanson, I. K. *Atlas of Point Contact Spectra of Electron-phonon Interactions in Metals* (Kluwer Academic, Dordrecht, 1995).
25. Ludoph, B. & van Ruitenbeek, J. M. Conductance fluctuations as a tool for investigating the quantum modes in atomic-size metallic contacts. *Phys. Rev. B* **61,** 2273–2285 (2000).
26. Frisch, M. J. *et al.* Gaussian 98, Revision A.5 (Gaussian, Inc., Pittsburgh, Pennsylvania, 1998).
27. Andrae, D., Häußermann, U., Dolg, M., Stoll, H. & Preuss, H. Energy-adjusted ab initio pseudopotentials for the 2nd and 3rd row transition-elements. *Theor. Chim. Acta* **77,** 123–141 (1990).
28. Becke, A. D. Density-functional thermochemistry. III. The role of exact exchange. *J. Chem. Phys.* **98,** 5648–5652 (1993).
29. Lang, N. D. Resistance of atomic wires. *Phys. Rev. B* **52,** 5335–5342 (1995).
30. Lang, N. D. & Avouris, Ph. Electrical conductance of individual molecules. *Phys. Rev. B* **64,** 125323 (2001).
31. Park, J. *et al.* Coulomb blockade and the Kondo effect in single-atom transistors. *Nature* **417,** 722–725 (2002).
32. Liang, W., Shores, M. P., Bockrath, M., Long, J. R. & Park, H. Kondo resonance in a single-molecule transistor. *Nature* **417,** 725–729 (2002).

Acknowledgements We acknowledge discussions with A. Levy Yeyati and S. K. Nielsen, and we thank D. Bakker and M. Pohlkamp for assistance in the experiments. C.U. and Y.N. were supported by European Community Marie Curie fellowships.

Competing interests statement The authors declare that they have no competing financial interests.

Correspondence and requests for materials should be addressed to J.M.v.R. (e-mail: ruitenbe@phys.leidenuniv.nl).

Relationship between local structure and phase transitions of a disordered solid solution

Ilya Grinberg, Valentino R. Cooper & Andrew M. Rappe

Department of Chemistry and Laboratory for Research on the Structure of Matter, University of Pennsylvania, Philadelphia, Pennsylvania 19104-6323, USA

The $Pb(Zr,Ti)O_3$ (PZT) disordered solid solution is widely used in piezoelectric applications owing to its excellent electromechanical properties. Six different structural phases have been observed for PZT at ambient pressure, each with different lattice parameters and average electric polarization. It is of significant interest to understand the microscopic origin of the complicated phase diagram and local structure of PZT[1–8]. Here, using density functional theory calculations, we show that the distortions of the material away from the parent perovskite structure can be predicted from the local arrangement of the Zr and Ti cations. We use the chemical rules obtained from density functional theory to create a phenomenological model to simulate PZT structures. We demonstrate how changes in the Zr/Ti composition give rise to phase transitions in PZT through changes in the populations of various local Pb atom environments.

PZT is a perovskite ABO_3 alloy with random B-site occupation by either Zr or Ti at all phases and compositions. The six structural phases that have been observed at ambient pressure are an antiferroelectric phase for compositions near $PbZrO_3$, ferroelectric low-temperature and high-temperature rhombohedral (R) phases for most Zr-rich alloys, a newly discovered monoclinic[2] (M) ferroelectric phase near 50% Zr/50% Ti ('50/50') composition, a tetragonal (T) ferroelectric phase for Ti-rich alloys, and a cubic paraelectric phase for all compositions at sufficiently high temperature. All phases of the material are generated by distortions from the same high-symmetry cubic parent structure, and are distinguished only by differing lattice parameters and by the directions of the structural distortions which give rise to the average polarization **P** of the material.

We have studied the local structure of PZT using *ab initio* density functional theory (DFT) calculations with the local density approximation (LDA) exchange-correlation functional. To obtain the ground-state structure, we minimize the energy with respect to ionic coordinates, starting with randomized perfect perovskite positions with no symmetry imposed. To represent the bulk nature of the material we use periodic boundary conditions. However, the disorder in the B-cation arrangement makes small, DFT-accessible supercells an inexact representation of the real material. This can be seen from the narrow peaks in the neutron scattering pair-distribution function (PDF) (representing the ensemble average distribution of interatomic distances in the crystal) of the DFT-obtained structure (Fig. 1). Increasing the size of the supercell

 © 2002 Nature Publishing Group